Supporting information

Manipulating charge-transfer kinetics and flow-domain LiF-rich interphase to enable high-performance microsized silicon-silver-carbon composite anode for solid-state batteries

Xiang Han[1], Lanhui Gu[1], Zhefei Sun[2], Minfeng Chen[1], Yinggan Zhang[2], Linshan Luo[3], Min Xu[1], Songyan Chen[3], Haodong Liu[5], Jiayu Wan[6], Yan-Bing He[4], Jizhang Chen[1,*], Qiaobao Zhang[2,7,*]

[1]*College of Materials Science and Engineering, Co-Innovation Center of Efficient Processing and Utilization of Forest Resources, Nanjing Forestry University, Nanjing 210037, Jiangsu, China*
[2]*State Key Laboratory of Physical Chemistry of Solid Surfaces, College of Materials, Xiamen University, Xiamen 361005, China*
[3]*Department of Physics, Xiamen University, Xiamen 361005, Fujian, China*
[4]*Shenzhen All-Solid-State Lithium Battery Electrolyte Engineering Research Center and Shenzhen Geim Graphene Center, Institute of Materials Research (IMR), Tsinghua Shenzhen International Graduate School, Tsinghua University, Shenzhen, China*
[5]*Chemical Engineering, UC San Diego, La Jolla, CA 92093, USA*
[6]*Department of Mechanical and Energy Engineering, Southern University of Science and Technology, Shenzhen, China*
[7]*Shenzhen Research Institute of Xiamen University, Shenzhen 518000, China*

*Corresponding authors: chenjizhang@njfu.edu.cn (J. Chen);
zhangqiaobao@xmu.edu.cn (Q. Zhang)

Methods

Materials synthesis

The micron-sized silicon (MSi) powders with an average diameter of ~ 1.5 μm was purchased from Xuzhou Lingyun Silicon Industry Co., Ltd. The MSi powders were directly put into an etching solution containing 0.02 M $AgNO_3$ and 5 M hydrofluoric acid (HF) at 50 °C and stirred for 30 min. To remove the residual solvent, the etching products were thoroughly washed by distilled water and EtOH for 5 times, respectively. After then, the as-obtained PS-Ag powders were dried in a vacuum oven at 80 °C for 6 h prior to use.

NASICON-type $Li_{1.3}Al_{0.3}Ti_{1.7}(PO_4)_3$ (LATP) was synthesized by a traditional solid-state reactive method. $LiOH \cdot H_2O$ (99.95%, Sigma Aldrich) (10% excessive), Al_2O_3 (99.99%, Sigma Aldrich), TiO_2 (99.98%, Sigma Aldrich), and $NH_4H_2PO_4$ (99.5%, Sigma Aldrich) were ground for 0.5 h in a mortar. The $LiOH \cdot H_2O$ powders were heated at 250 °C for 3 h to remove crystalline H_2O. Subsequently, the mixed powders were cold pressed into pellets with a diameter of 13 mm at 400 MPa. The pellets were then preheated at 400 °C in the air for 5 h, hand-ground into fine powders, cold-pressed into pellets, and sintered at 900 °C for 5 h. The as-synthesized LATP pellet was ball milled (600 r min^{-1} for 5 h) into nanoparticles.

For the preparation of poly (vinylidene fluoride)-co-hexafluoropropylene (PVDF-HFP) /LATP composite SSE, the 0.6 g PVDF-HFP powders, 0.6 g lithium bis (trifluoromethane sulfonimide) (LiTFSI) and 0.2 g LATP nanoparticles were dissolved in DMF and stirred at 60 °C for 24 h. After then, the slurry was cast on a clean glass plate, PVDF-HFP/LATP solid-state composite SSE film was fabricated after dried in a vacuum oven at 60 °C for 24 h. The thickness of the prepared film PVDF-HFP/LATP SSE is ~ 50 μm.

Physicochemical characterizations

The crystal structures of the as-synthesized LATP, MSi, PS-Ag and SSE were detected by X-ray diffraction (XRD) (Cu K_α, λ ~ 0.15406 nm). A field-emission scanning electron microscope (FESEM, JSM-7600F) was applied to observe the

surface and cross-sectional morphology of the PS-Ag particles and PS-Ag-C electrode. The microstructures and chemical compositions of PS-Ag-C before and after cycling were analyzed by a transmission electron microscope (TEM) equipped with energy-dispersive X-ray spectroscopy (EDS) (FEI Titan F20). The nitrogen adsorption and desorption isotherm were tested at 77 K in a range of relative pressure of 0.0001–0.99 P/P_0 using a TriStar II surface area and porosity system (Micromeritics).

The cryo-TEM image and corresponding electron energy loss spectroscopy (EELS) spectra of SEI information was conducted by HRTEM (Aztec, Oxford Instruments). The surface chemistry was analyzed by X-ray photoelectron spectroscopy (XPS) (Thermo Scientific K_α spectrometer). ToF-SIMS measurements were carried out on a PHI nanoTOF II with a Bi^+ source. Sputtering with an Ar^+ ion beam (3 keV, 100 nA) was performed for the depth profile analysis in a 400×400 μm^2 area. Atomic force microscopy (AFM) was performed on Bruker Dimension Icon (Germany) in an area of $5 \times 5 \mu m^2$. Inductive coupled plasma atomic emission spectrometer (ICP-AES) was carried out on a PerkinElmer 8300. Thermal gravimetric analysis (TGA) was performed on Netzsch STA 449 F3. The volume expansion of PS-Ag-C full cell was tested on Model Coin Cell System (MCS1000, IEST) with a height accuracy of 0.1 μm.

In situ TEM observation

The live lithiation/delithiation process of PS-Ag-C was conducted in a TEM with Nanofactory TEM-STM holder. The PS-Ag-C was loaded on the Mo tip and then contact with Li source that is mounted on a W tip. In this configuration, the naturally formed Li_2O on the surface of Li metal served as solid electrolyte facilitating the diffusion of Li^+. Lithiation process of PS-Ag-C was initiated by applying a positive voltage (+3V) on Li/Li_2O end. Once the lithiation process finished, a reverse voltage (-3V) was applied to the Li/Li_2O to start the delithiation process. In addition, in order to minimize the side effect of electron beam on experiment, the electron dosage of all the tests was controlled below 1 A cm^{-2}.

In situ XRD measurement

In situ XRD test of PS-Ag-C anode was conducted on a Bruker D8 Advance machine with Cu Kα as the X-Ray source) with lithium foil as the counter electrode and PS-Ag-C with a loading of 8 mg cm^{-2} serving as work electrode in a specially designed cell during the first charging and discharging process. After the cell was rested for 6 hours, it was then discharged and charged between the voltage window 0.005 and 1.5 V at 0.05 A g^{-1} on a LAND multichannel battery tester (CT2001A) with the simultaneous collection of the phase changes of PS-Ag-C anode.

Electrochemical performance evaluation

For the preparation of PS-Ag-C electrode, the PS-Ag powders and polyacrylonitrile (PAN) solution (10 wt.% dissolved in N, N-Dimethylformamide (DMF)) were mixed in a weight ratio of 7:3 and ball-milled 2 h to form a slurry. The mixed slurry was spread onto copper foil and dried for 12 h in a vacuum drying oven at 80 °C to evaporate the residual DMF. The as obtained PS-Ag-PAN on copper foil was cut into small discs with a diameter of 12 mm and then calcined at 700 °C for 2 h under Ar/H$_2$ (5%) atmosphere to obtain the PS-Ag-C electrode. The mass loading determined in our manuscript is the total mass of PS-Ag-C electrode (including Cu disc current collector) minus the mass of Cu foil, which was precisely weighed by a microbalance (METTLER TOLEDO XS3DU) with an accuracy of 1 μg. The active material mass loading including PS, Ag and C is $0.5 - 2.3$ mg cm^{-2}.

All the electrochemical performances were tested in CR 2025-type coin cells, which were assembled in a glovebox filled with high purity Ar (H$_2$O< 1 ppm, O$_2$< 1 ppm). The electrolyte used in liquid cell was 1 M LiPF$_6$ in ethylene carbonate (EC)/dimethyl carbonate (DMC)/diethyl carbonate (DEC) (1:1:1 by volume) with the addition of 10 vol. % fluoroethylene carbonate (FEC). The coil cells were measured between 0.005 and 1.5 V on a LAND CT2001A battery test instrument. Cyclic voltammetry (CV) with a scan rate of 0.2 mV s^{-1} was performed on a Bio-Logic VSP-300 electrochemical workstation. Electrochemical impedance spectroscopy (EIS) tests were carried out between 7 MHz and 0.1 Hz with an alternating current (AC) amplitude

of 10 mV to record the impedance variation of PS-Ag-C anode during cycling.

Ionic conductivity (σ) of LATP/PVDF-HFP SSE was calculated based on the following formula:

$$\sigma = \frac{L}{RS} \tag{1},$$

where L is the thickness of solid polymer electrolyte; R is the high-frequency intercept obtained from the electrochemical impedance spectroscopy (EIS); S is the surface area of the electrode. The calculation formula of the lithium-ion migration number (t^+) can be expressed as follows [1]:

$$t^+ = \frac{I_{ss}(\Delta V - I_0 R_0)}{I_0(\Delta V - I_{ss}R_{ss})} \tag{2},$$

where ΔV is the applied polarization voltage; I_0 and I_s are the initial current and steady-state current, respectively; R_0 and R_{ss} are the initial resistance and steady-state resistance, respectively. Usually, a metal lithium symmetrical electrode is sandwiched with composite solid electrolytes to form a 2025 coin-type half-cell, which is tested by the AC impedance and potentiostatic chronoamperometry. For the AC impedance test, the frequency range is set as 0.01 Hz − 7 MHz, and the amplitude of the voltage is set as 10 mV. The I−t curve was obtained by the Bio-Logic VSP-300 electrochemical workstation and potentiostatic chronoamperometry, where ΔV was 10 mV; time t was 7200 s; the test temperature was 50 °C.

To assemble the solid-state half-cell, the PVDF-HFP/LATP SSE serves as separator and electrolyte between PS-Ag-C electrode and lithium metal. Full cells were fabricated by pairing PS-Ag-C anode material and Li (Ni$_{0.8}$Co$_{0.1}$Mn$_{0.1}$) O$_2$ (NCM, purchased from Canrd) cathode. The cathode was composed of 80 wt.% NMC811, 10 wt.% carbon black, and 10 wt.% poly (vinylidene fluoride) (PVDF). The capacity ratio of PS-Ag-C to NCM was ~ 1.1:1. The mass loading of PS-Ag-C in full cell is 0.5 mg cm^{-2}. The specific capacity of the full cells was measured at 1 A g^{-1} (based on PS-Ag-C) between 2.5 and 4.4 V. The electrochemical cycling performances of all solid-state cells were performed at 50 °C.

Computational methods

All the density functional theory calculations were performed using Vienna ab initio simulation package (VASP) [2,3] with Pwedew-Burke-Ernzerhof (PBE) [4] functional of the generalized-gradient approximation (GGA) to the exchange-correlation potential. Projector augmented-wave method (PAW) was used, and the plane wave basis set was cut off at the energy of 500 eV. The k-points of 9×9×1 automatically generated by the Monkhorst-Pack scheme were adopted in the Brillouin zone and a vacuum layer of 20 Å was set in present calculations. The Li diffusion barrier energies were calculated by climbing-image nudged elastic band method (CI-NEB) [5].
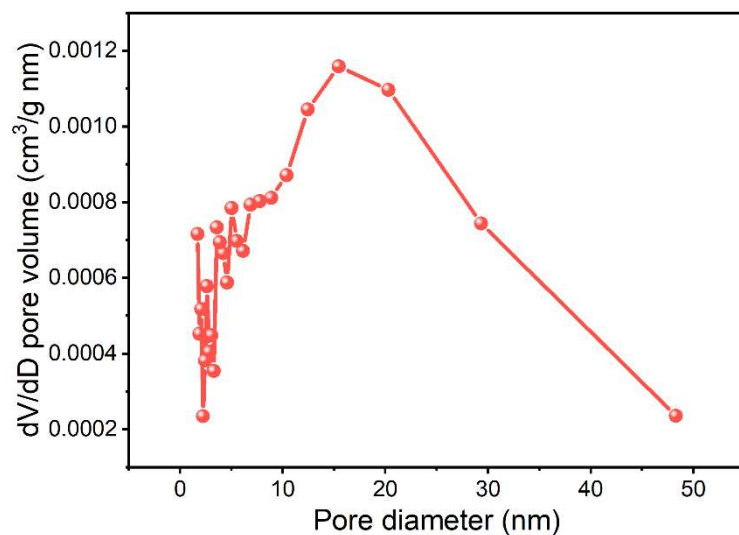
Figure. S1 BET pore size distribution for PS-Ag.
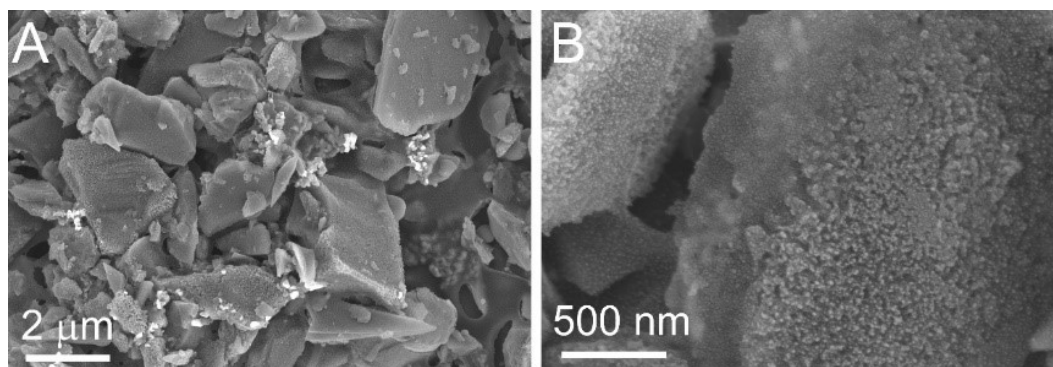
Figure.S2 (A) Surface SEM image of PS-Ag-C electrode. (B) A high magnification view in (A).
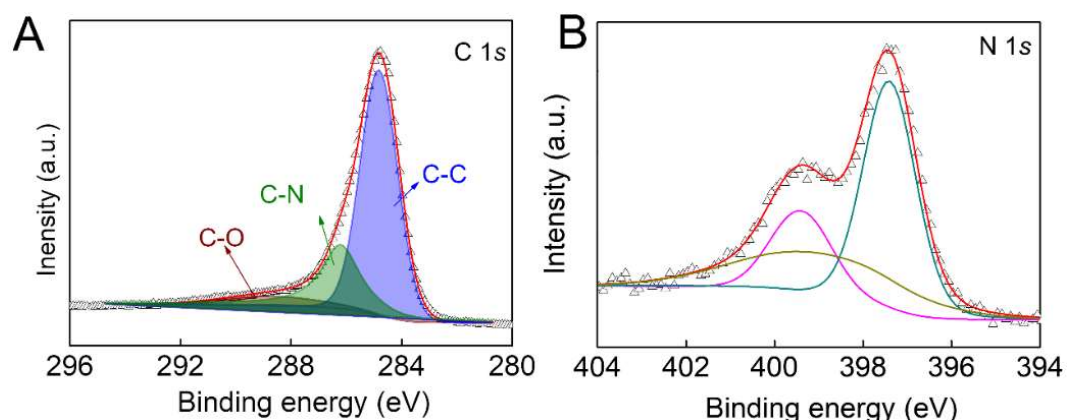
Figure.S3 High resolution XPS spectra of PS-Ag-C electrode: (A) C 1s, (B) N 1s.
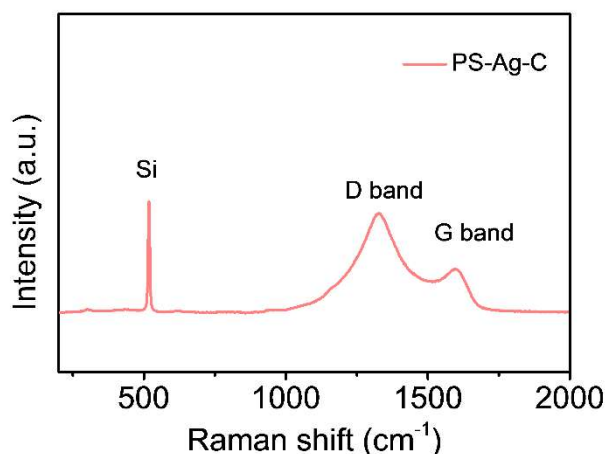
Figure. S4 Raman spectrum of PS-Ag-C electrode.
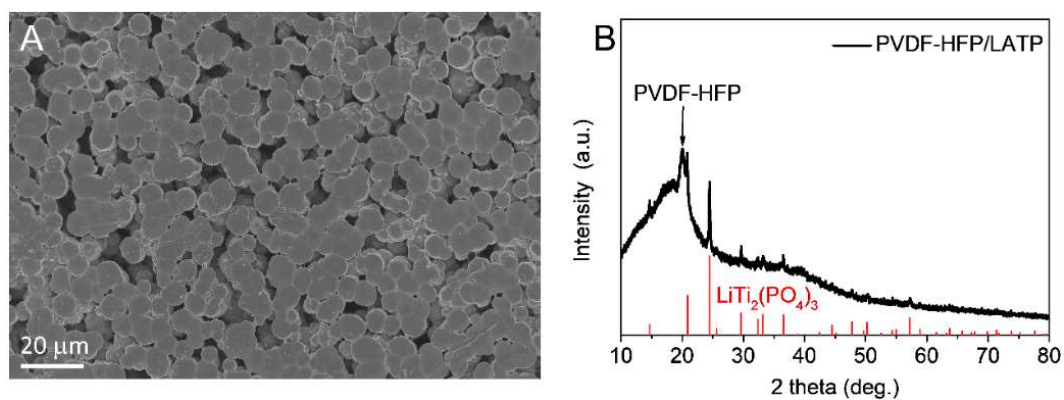
Figure. S5 (A) Surface SEM image of PVDF-HFP/LATP SSE. (B) XRD patterns of PVDF-HFP/LATP SSE.
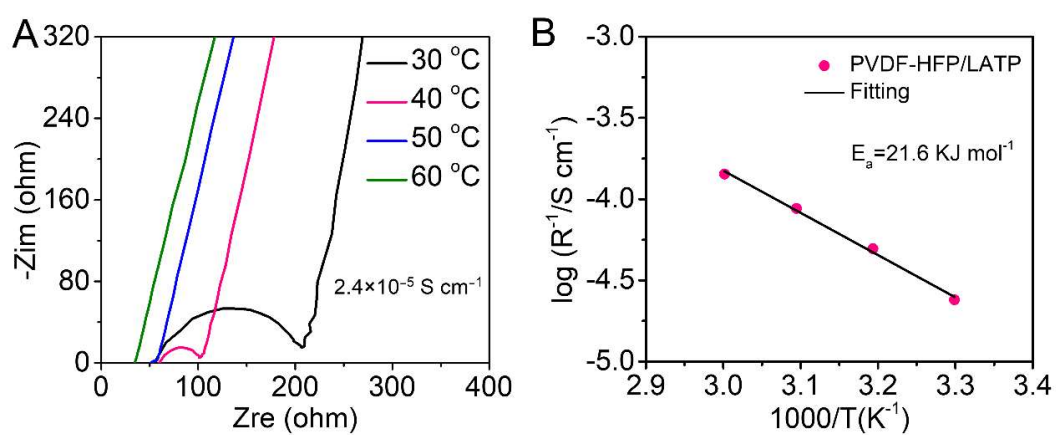
Figure. S6 (A) EIS spectra of PVDF-HFP/LATP SSE in a temperature window of 30-60 °C. (B) Arrhenius plot of conductivity for PVDF-HFP/LATP SSE.
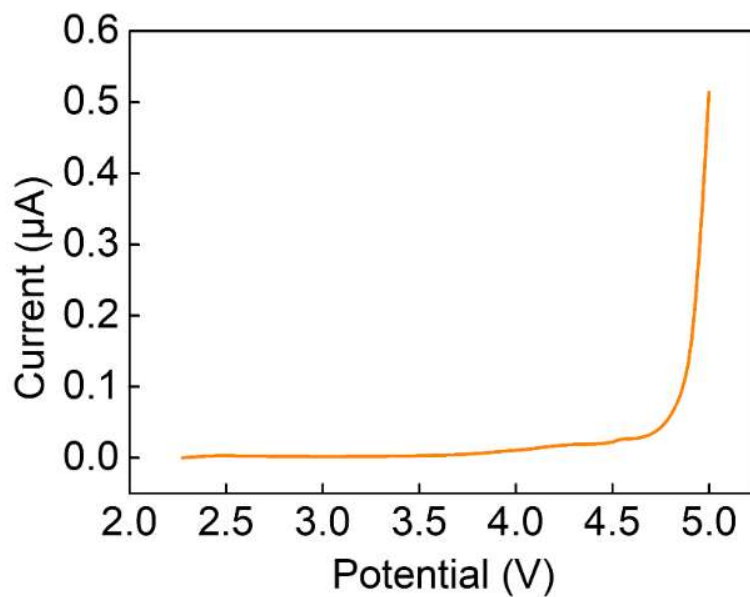
Figure. S7 Linear sweep voltammetry of PVDF-HFP/LATP SSE.
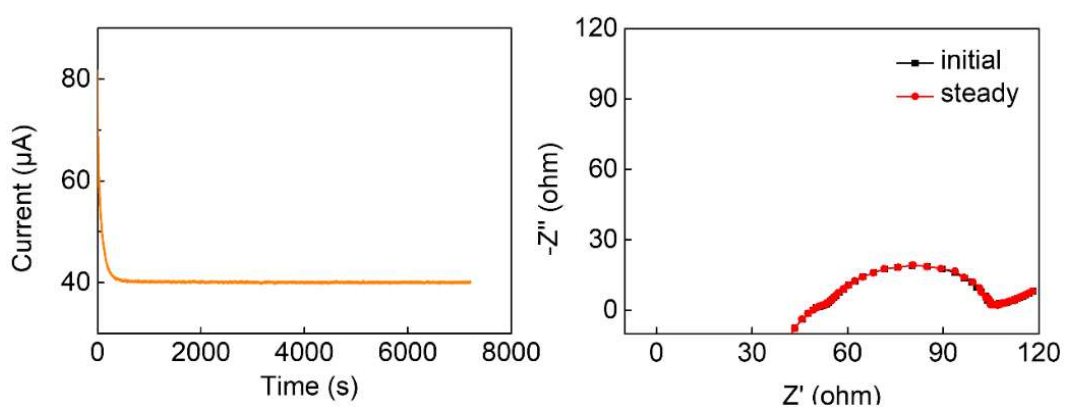
Figure. S8 (A) Current-time curve obtained from chronoamperometry at a DC polarization of 0.01 V. (B) EIS response of the cell before and after polarization.
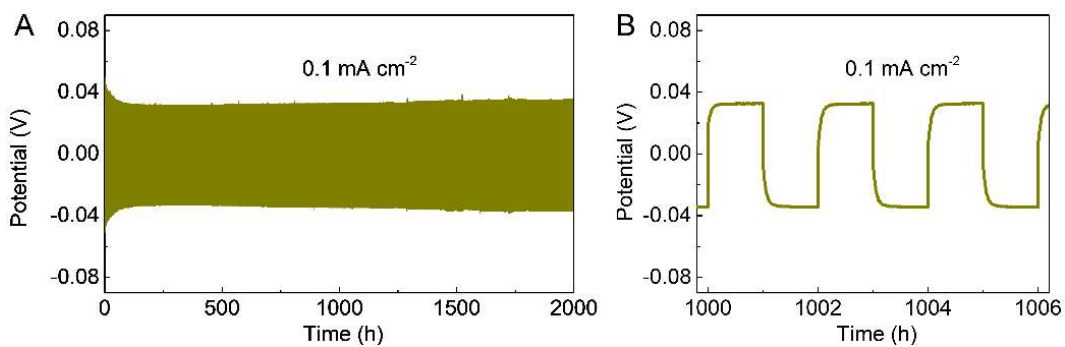
Figure. S9 (A) Voltage profiles of Li-Li symmetric cell used PVDF-HFP/LATP SSE. (B) Enlarged voltage profile in (A)
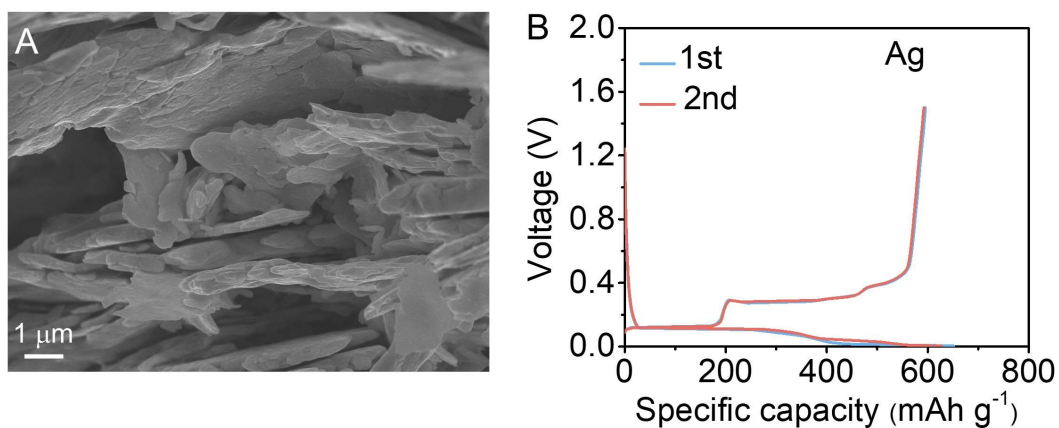
Figure S10. SEM images of Ag flakes used for electrochemical performance test. (B) The charge-discharge profiles of Ag electrode at 0.2 A/g between 0.005 and 1.5 V.

PS-Ag	HF+H_2O_2 dissolved	Diluted 10 times	Ag content
10 mg	100 mL	Ag^+ content 8.6 mg/L	8.6%
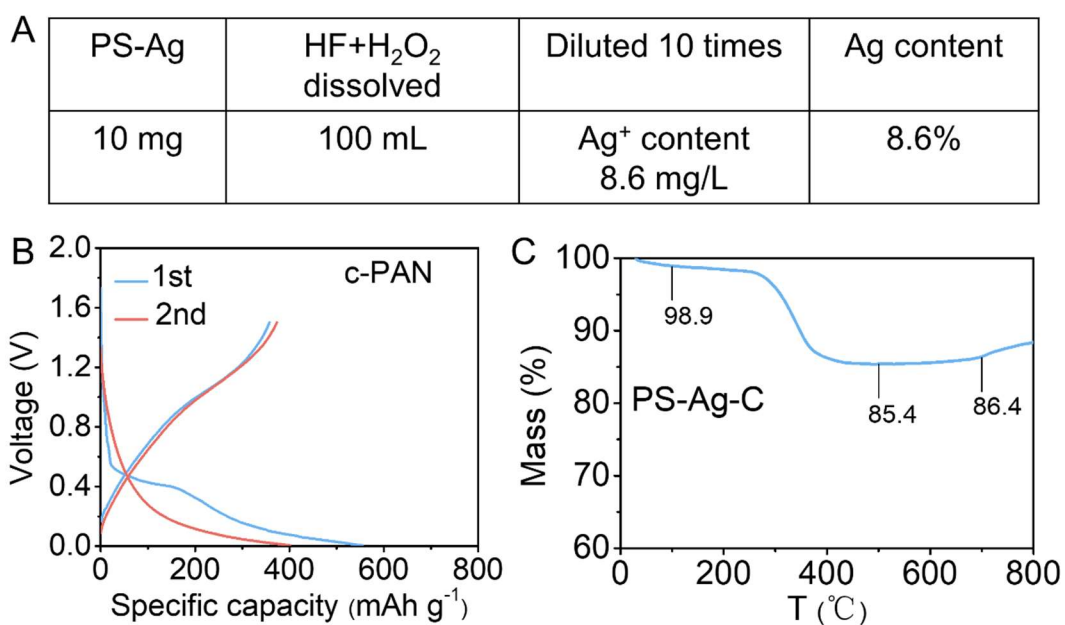
Figure S11. (A) The result of Ag content in PS-Ag measured by inductively coupled plasma atomic emission spectroscopy (ICP-AES). (B) The charge-discharge profile of carbonized PAN. (C) TG curve of PS-Ag-C powders measured by thermal gravimetric analysis (TGA).
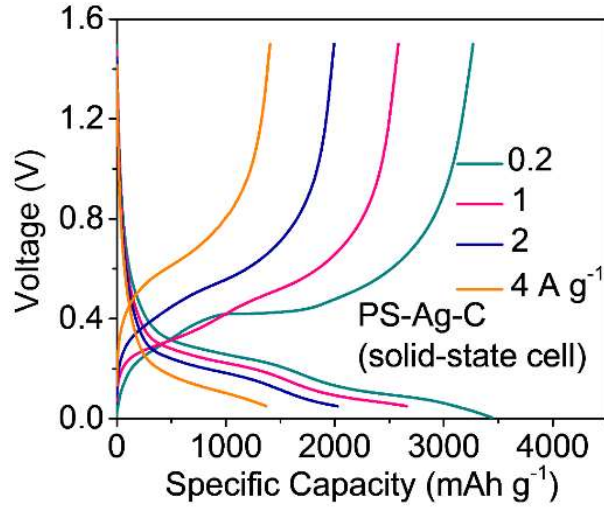
Figure. S12 Charge-discharge voltage profiles of PS-Ag-C electrode at various current density.
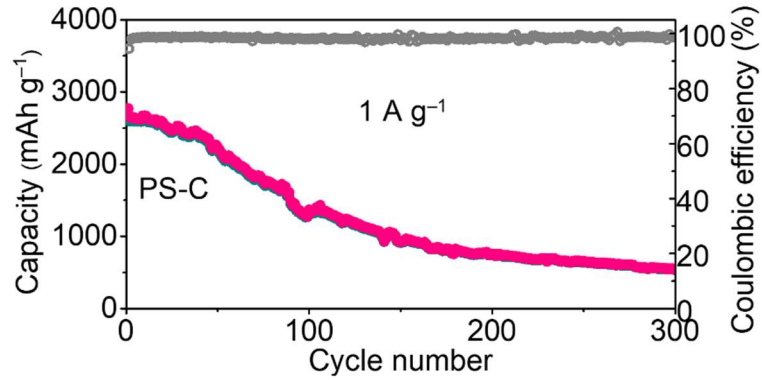
Figure S13. The cycling performance of PS-C electrode in a solid-state cell at 1 A g^{-1}.
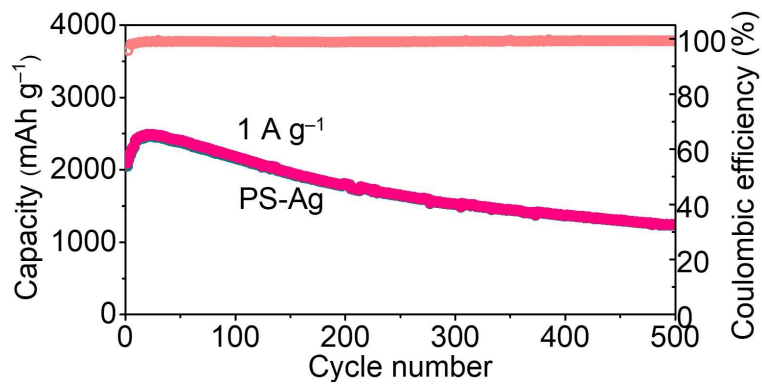
Figure S14. The cycling performance of PS-Ag electrode a solid-state cell at 1 A g^{-1}.
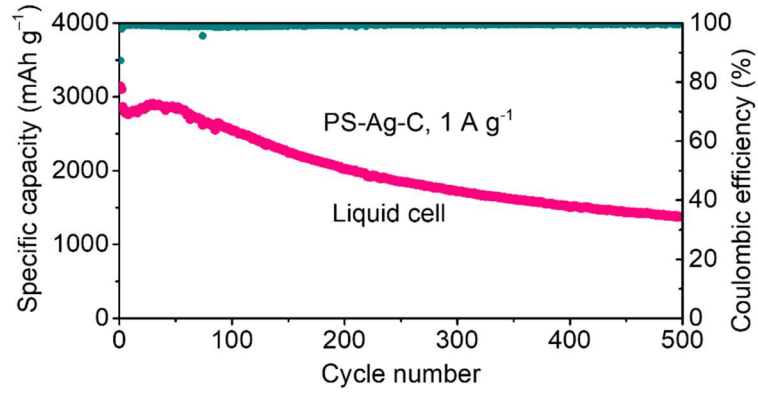
Figure S15. Cycling performance of PS-Ag-C electrode in a liquid electrolyte cell at 1 A g^{-1}.
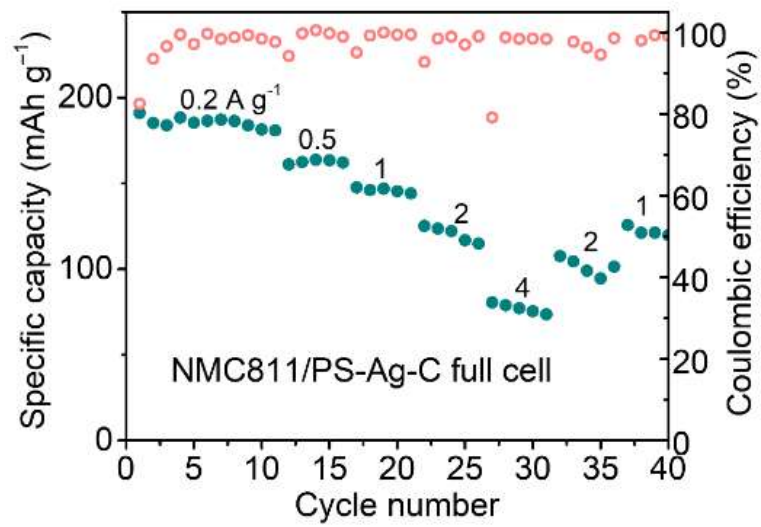

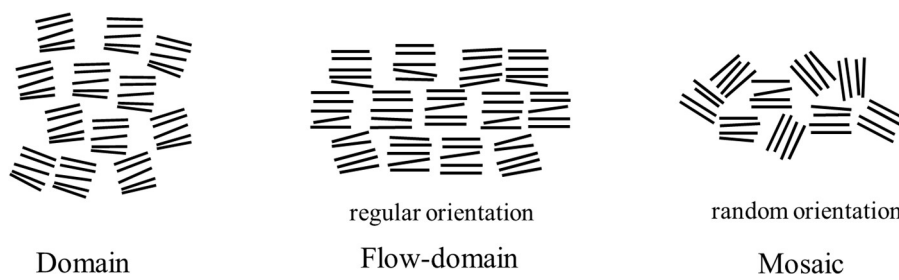Figure S16. Rate performance of solid-state NMC811/PS-Ag-C full cell.

Figure S17. The schematic illustration of domain, flow domain and mosaic structure.
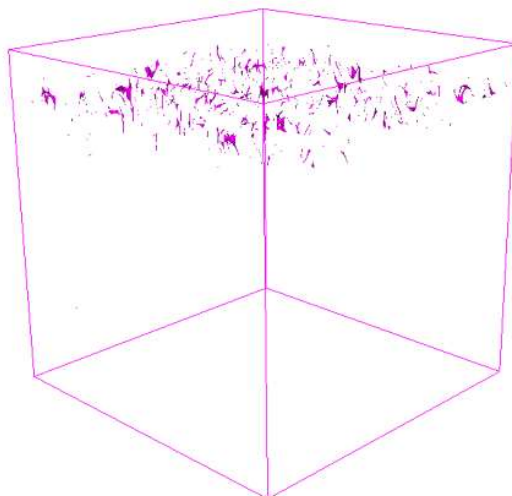
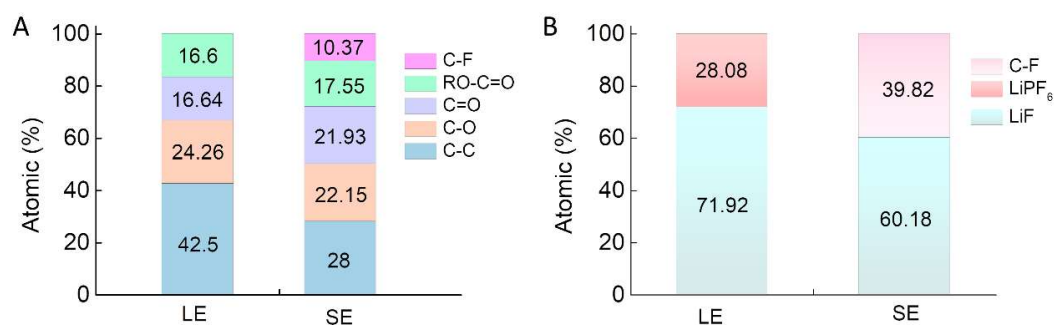Figure S18. 3D map showing the distribution of $LiCO_3^-$ for PS-Ag-C anode in a solid-state cell.

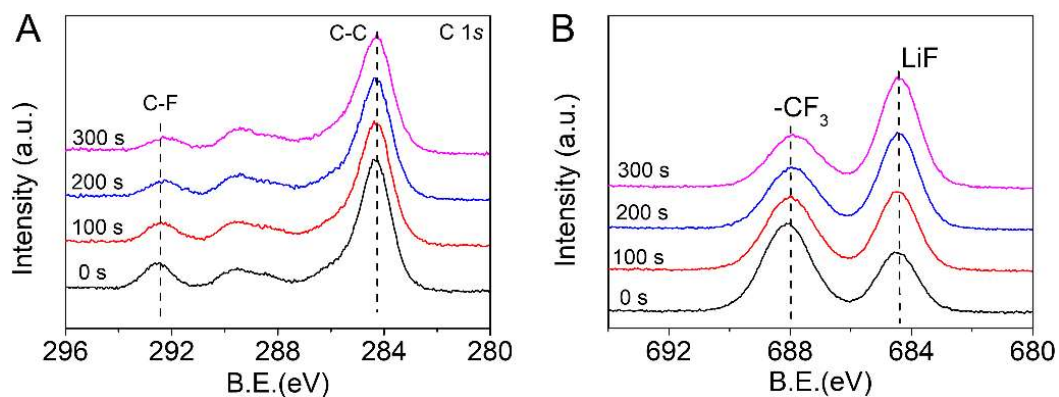Figure. S19 The detailed content ratio of different components in the SEI layer for liquid and solid cells.

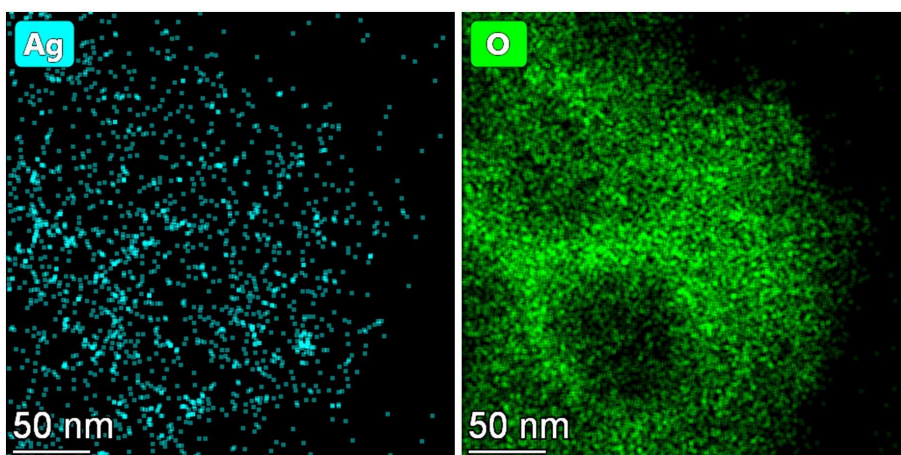Figure S20. (A) XPS depth profiles of C 1*s* spectrum. (B) XPS depth profiles of F 1*s* spectrum.

Figure S21. EDS elemental mapping of PS-Ag-C electrode after long-term cycle in a solid-state cell.
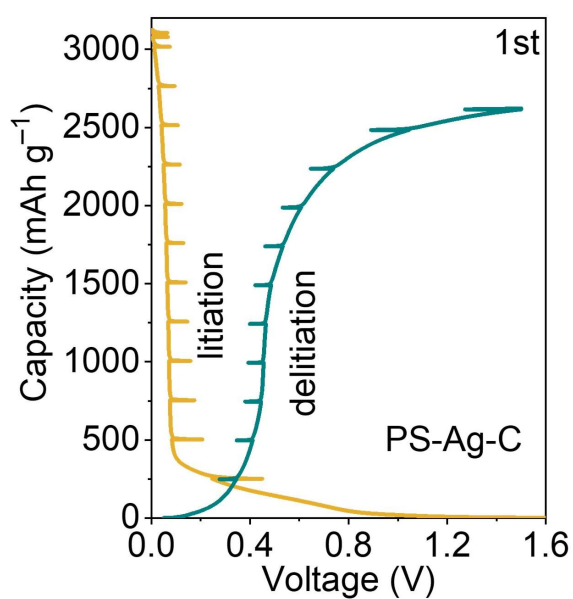

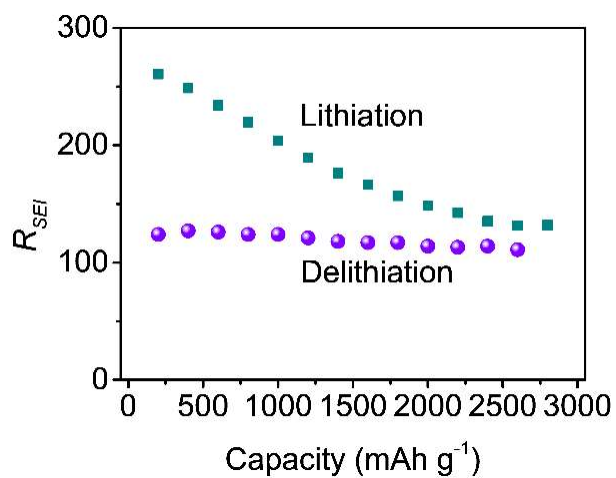Figure S22. The charge and discharge curve of PS-Ag-C electrode during *in situ* EIS test.

Figure S23. The fitting results of SEI resistance for a PS-Ag-C electrode during the initial cycle.
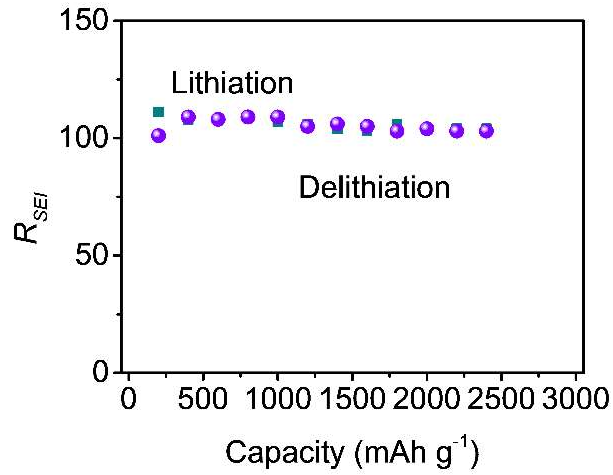
Figure 24. The fitting results of SEI resistance for a PS-Ag-C electrode during the second cycle.
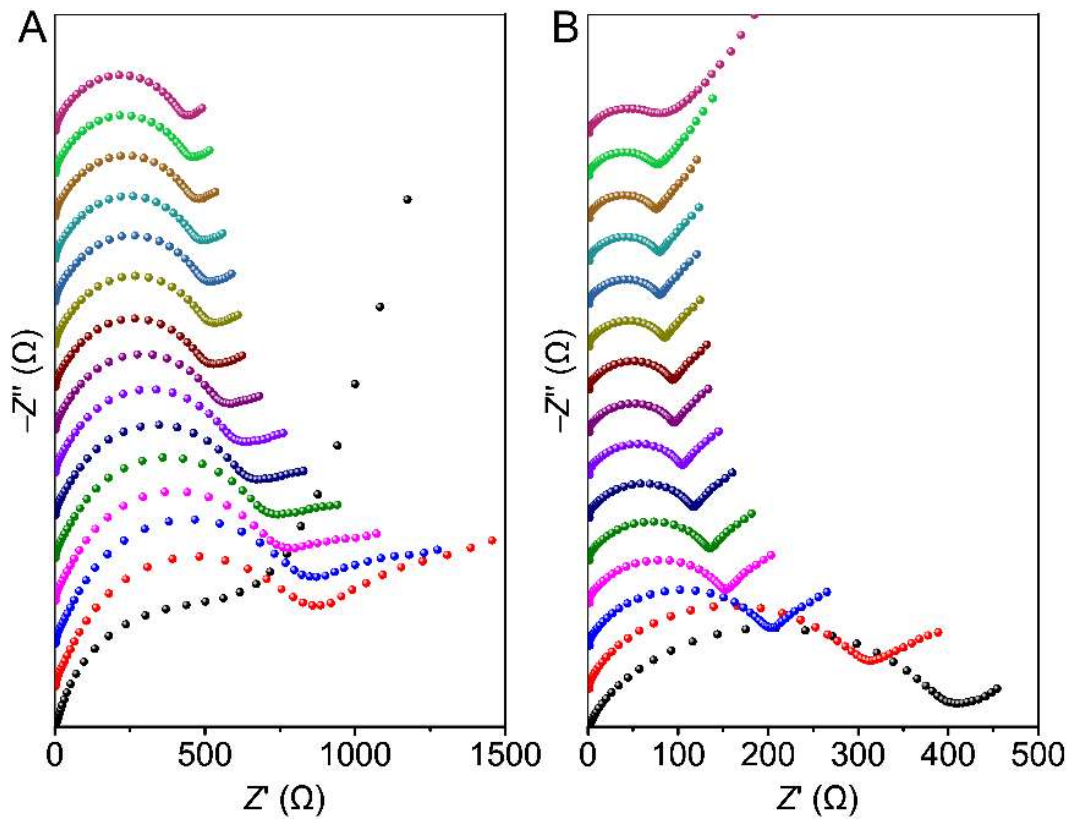

Figure S25. (A) The EIS spectra variation of PS-Ag-C anode in a liquid cell during the initial lithiation process. (B) The EIS spectra variation of PS-Ag-C anode in a liquid cell during the initial delithiation process.
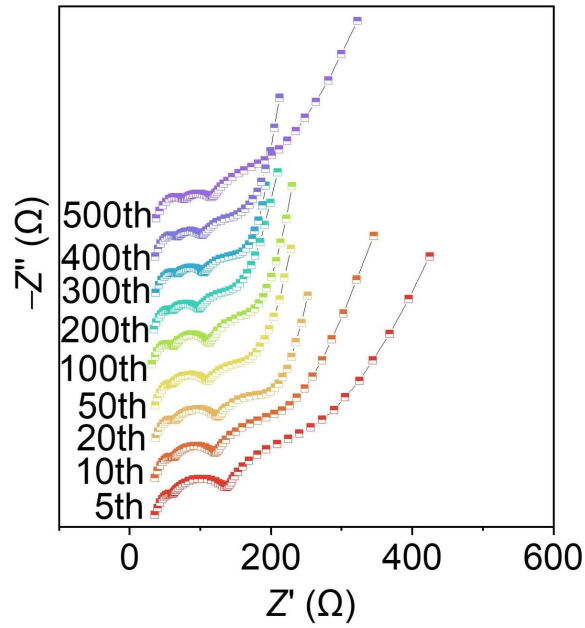
Figure S26. The EIS impedance spectra of PS-Ag-C collected during various cycles.
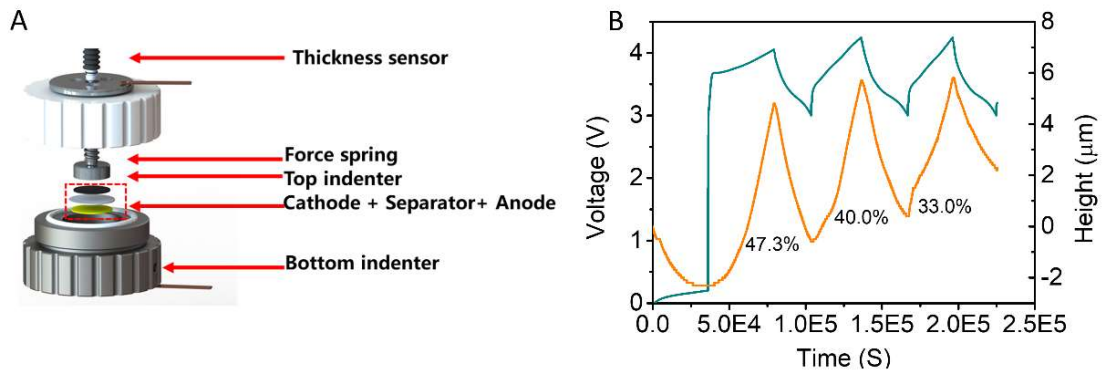

Figure S27. (A) The schematic illustration of the model coin cell system. (B) Volume expansion of the PS-AG-C full cell during the first three cycles.
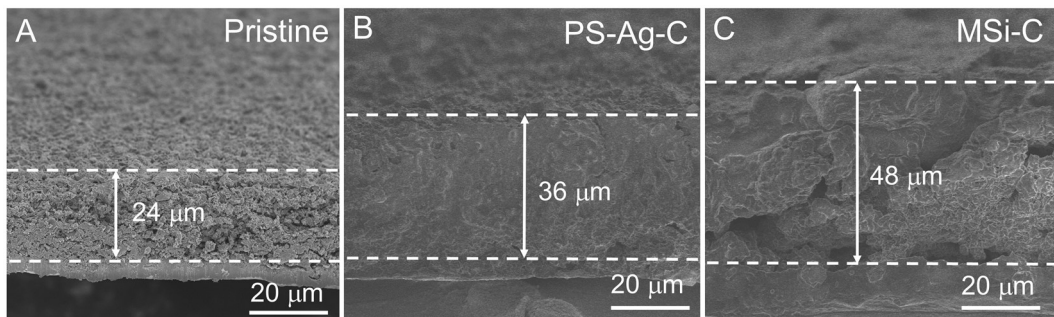

Figure S28. (A) Cross sectional SEM image of pristine PS-Ag-C electrode. (B) Cross sectional SEM image of PS-Ag-C electrode after first lithiation. (C) Cross sectional SEM image of MSi-C electrode after first lithiation.
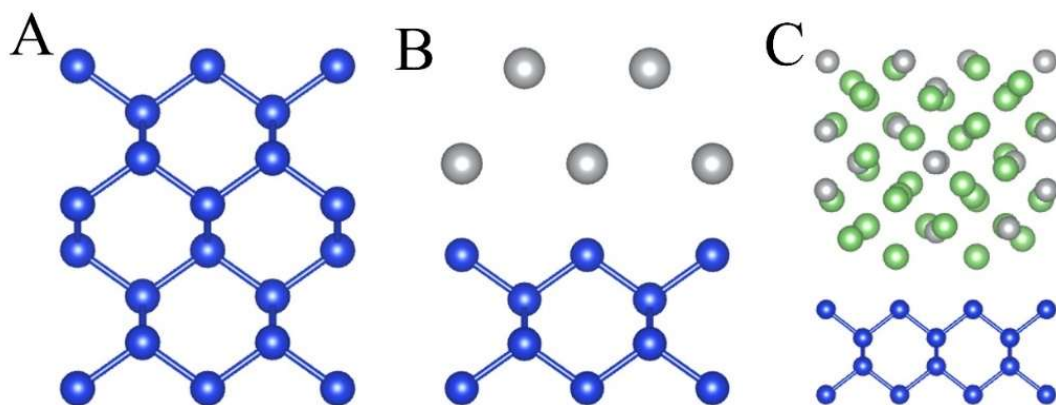
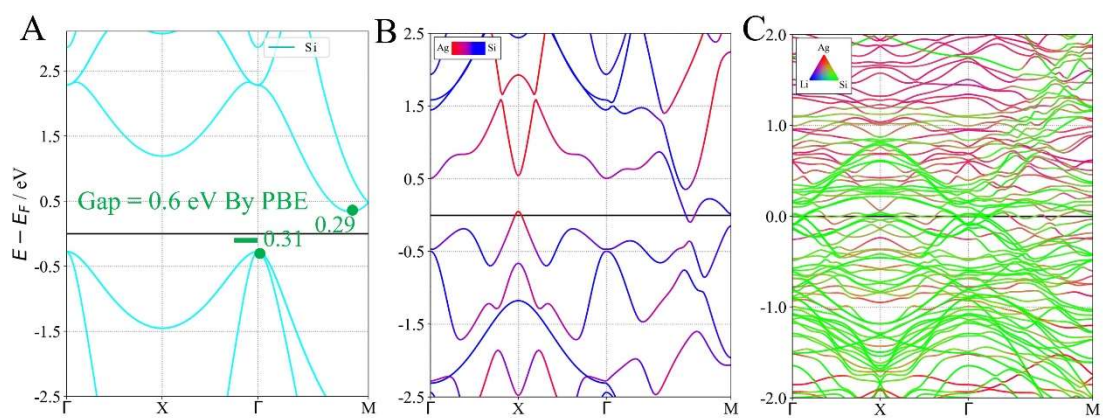Figure S29. Side views of diffusion pathways of Li atom for (a) Si and (b) Si/Ag structures.

Figure S30. The calculated band structures of (A) Si, (B) Si/Ag and (C) Li$_9$Ag$_4$/Si.
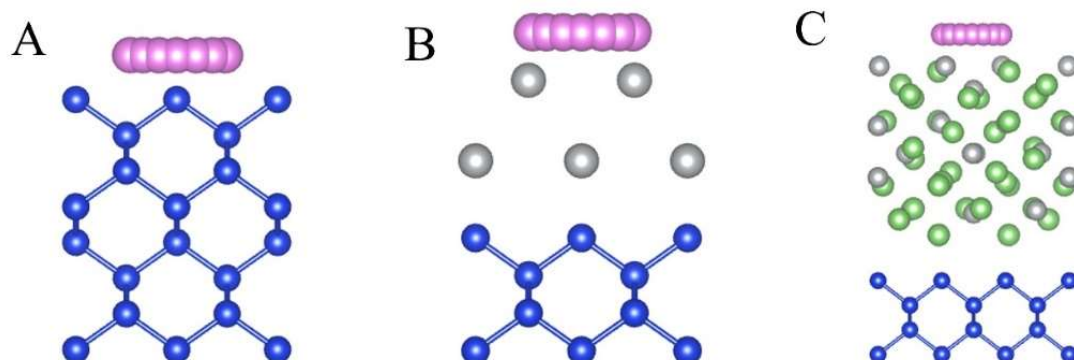

Figure S31. Side views of diffusion pathways of Li atom for (A) Si, (B) Si/Ag and (C) Li$_9$Ag$_4$/Si.

Table S1. The performance comparisons of PS-Ag-C anode with previously reported results of Si anodes in solid-state batteries

	Mass loading (mg/cm²)	Areal capacity (mAh/cm²)	Cycle number	ICE (%)	Specific capacity (mAh/g)
Our work	**2**	**4.4**	**500**	**89**	**3030**
Ref. 6	0.23	0.6377	200	85.6	2773
Ref. 7	0.7	1.75	300	82.7	2500
Ref. 8	0.23	0.598	140	95	2600
Ref. 9	1	3.5	100	84	2912
Ref. 10	0.05	1.35	100	54	2702
Ref. 11	0.74	2	375	90	3059
Ref. 12	0.1	2.52	200	68	2520

Captions of Supplementary Movies

Movie S1: *In situ* TEM observation of lithiation/delithiation of a PS-Ag electrode for 3 cycles at high magnification (the display was sped up by 20 times the real time of lithiation).

Movie S2: *In situ* TEM observation of lithiation/delithiation of a PS-Ag electrode for 2 cycles at low magnification (the display was sped up by 200 times the real time of lithiation).

References

1. Chai J, *et al*. In situ generation of poly (vinylene carbonate) based solid electrolyte with interfacial stability for $LiCoO_2$ lithium batteries. *Adv. Sci.* **4**, 1600377 (2017).

2. G. Kresse, J. Furthmüller. Efficient iterative schemes for ab initio total-energy calculations using a plane-wave basis set. *Phys. Rev. B* **54**, 11169 (1996).

3. G. Kresse, D. Joubert. From ultrasoft pseudopotentials to the projector augmented-wave method. *Phys. Rev. B* **59**, 1758 (1999).

4. J.P. Perdew, K. Burke, M. Ernzerhof. Generalized gradient approximation made simple. *Phys. Rev. Lett.* **77**, 3865 (1996).

5. G. Henkelman, B.P. Uberuaga, H. Jónsson. A climbing image nudged elastic band method for finding saddle points and minimum energy paths. *J. Chem. Phys.* **113**, 9901-9904 (2000).

6. Cangaz S, *et al.* Enabling high-energy solid-state batteries with stable anode interphase by the use of columnar silicon anodes. *Adv. Energy Mater.* **10**, 202001320 (2020).

7. Cao D, Sun X, Li Y, Anderson A, Lu W, Zhu H. Long-cycling sulfide-based all-solid-state batteries enabled by electrochemo-mechanically stableelectrodes. *Adv. Mater.* **34**, e2200401 (2022).

8. Cao D, Sun X, Wang Y, Zhu H. Bipolar stackings high voltage and high cell level energy density sulfide based all-solid-state batteries. *Energy Storage Mater.* **48**, 458-465 (2022).

9. Ferraresi G, El Kazzi M, Czornomaz L, Tsai C-L, Uhlenbruck S, Villevieille C. Electrochemical performance of all-solid-state li-ion batteries based on garnet electrolyte using silicon as a model electrode. *ACS Energy Lett.* **3**, 1006-1012 (2018).

10. Huo H, *et al.* Flexible interfaces between Si anodes and composite electrolytes consisting of

poly(propylene carbonates) and garnets for solid-state batteries. *J. Power Sources* **383**, 150-156 (2018).

11. Ryu J*, et al.* Room-temperature crosslinkable natural polymer binder for high-rate and stable silicon anodes. *Adv. Funct. Mater.* **30**, 201908433 (2019).

12. Yamamoto M, Terauchi Y, Sakuda A, Takahashi M. Slurry mixing for fabricating silicon-composite electrodes in all-solid-state batteries with high areal capacity and cycling stability. *J. Power Sources* **402**, 506-512 (2018).